# Chapter 8
# Fréedericksz-Like Positional Transition Triggered by An External Electric Field

**Ke Xiao and Chen-Xu Wu**

**Abstract** Microparticles (colloidal particles) of different shapes suspended in an anisotropic nematic liquid crystal (NLC) host medium are important soft matter systems which behave quite differently from those simply composed of microparticles or conventional isotropic liquids. The embedded microparticles disturb the alignment of LC molecules and induce elastic distortions, generating long-range anisotropic interactions and topological defects. The replacement of isotropic liquids with NLC medium gives rise to abundant physical behaviors of the microparticles, which leads to a broad range of practical applications ranging from biological detectors to new display and topological memory devices. This chapter is devoted to the new dynamic behaviors of a microparticle suspended in a uniform nematic liquid crystal (NLC) cell in the presence of an external electric field, an important tool in soft matter systems to manipulate microparticles. Investigating the basic dependence of critical electric value on cell thickness, Frank elastic constant, microparticle size and density is essential for understanding the dynamical behaviors of micropartices. This chapter is organized as follows. We start with a short introduction on liquid crystal together with a review of the related literature on microparticle-suspended liquid crystal (Sect. 8.1). The theoretical background of liquid crystals with particular focus on order parameter, Frank-Oseen free energy, surface anchoring free energy, Fréedericksz transition, and multipole expansion is described in Sect. 8.2. The main theoretical model and tools are then outlined in Sect. 8.3 to study the properties of a single particle in a uniform nematic liquid crystal cell in the presence of an external electric field. The main results and discussions based on the theoretical model we proposed in Sect. 8.3 are presented in Sect. 8.4. In Sect. 8.5 a brief summary is made.

**Keywords** Nematic liquid crystal · Positional transition · Effective elastic energy · Green's function method

K. Xiao · C.-X. Wu (✉)
Department of Physics, College of Physical Science and Technology, Xiamen University, Fujian, People's Republic of China
e-mail: cxwu@xmu.edu.cn



X.-Y. Liu (ed.), *Frontiers and Progress of Current Soft Matter Research*,
Soft and Biological Matter, https://doi.org/10.1007/978-981-15-9297-3_8

## 8.1 Introduction

Liquid crystals (LCs) are soft materials made of organic molecules with rodlike, disclike or banana shapes, a mesophase intermediate between the crystalline and isotropic liquid state formed at a certain temperature or molecular concentration range [1, 2]. In the undeformed ground state, uniaxial molecules in nematic liquid crystal (NLC) phase, the simplest type of all orientational orders, prefer an orientation with their molecular long axes aligning along a common direction **n** called director. It is widely accepted that the NLCs possess many anisotropic physical properties that are easy to control by external stimuli owing to their long-range orientational order rather than translational order. Colloids, which are widely used in our daily life, including milk, ink, paint, cream and fog, are dispersions of solid, liquid or gas particles with typical size ranging from a few nanometers up to a few micrometers in a host surrounding medium [3, 4]. When dispersed in a NLC, the colloidal particles disturb the alignment of LC molecules and induce elastic distortions which give rise to long-range anisotropic interactions and topological defects. The generated long-range force leads to the self-assembly of molecules in such system, a topological phenomenon offering the possibility to control and design anticipated function for novel composite materials and diverse topology materials with similar features. One of the main themes of liquid crystal is to study the properties and behaviors of colloids suspended in nematic liquid crystal (NLC), and a wide range of promising practical applications have been realized, such as new display and topological memory devices [5–7], new materials [8], external triggers and release microcargo [9], and biological detectors [10, 11]. Over the past two decades, many experimental, theoretical and computer simulation studies have been focused on the physical properties of colloidal particles embedded within NLCs [12–25].

At the experimental level, diverse methods and techniques have been developed to measure the interaction force between particles in NLC in a direct manner [12, 26–29]. It has been found that the interaction force of spherical particles suspended in NLC is associated not only with interparticle distance and geological confinement [13], but also with the shape of particles which plays a crucial role in pair interaction and aggregation behaviors [17]. Whereas, in the presence of the electric field, fruitful fascinating physical phenomena such as levitation, lift, bidirectional motion, aggregation, Electrokinetic and superdiffusion [24, 30–32] have been observed for colloids dispersed in NLCs. On the other hand, theoretical modeling and computer simulation as useful complements to experiments, such as Landau-de Gennes (LdG) theory and elastic free energy method, have been carried out to interpret the nature of colloidal particles dispersed in NLCs. Generally Monte Carlo simulation [23, 33], lattice Boltzmann method [34, 35] and finite element method [13, 36–39] are common adopted techniques to minimize the LdG free energy functional. Except for the methods mentioned above, recently S. B. Chernyshuk and coauthors studied the interaction between colloidal particles in NLCs with or without external field by using Green's function method, and obtained general formulae for interaction energy between colloidal particles [40–42]. In the liquid crystal and particles coex-

istence system, it is observed that external field is able to drive particles apart [12], cause rotation [18] and alignment [43] of LC molecules, and even manipulate the equilibrium position of microdroplet [44]. Although interactions of two particles in a NLC are very well understood and the particle-wall interaction has been widely observed experimentally for a single particle immersed in a nematic cell [41, 45, 46], the properties of a single particle in a uniform NLC cell in the presence of an external electric field theoretically have not been fully addressed. Thus, it is of crucial importance to investigate the nature of a single particle in a uniform NLC cell in the presence of an external electric field.

## 8.2 Fréedericksz Transition in NLC

In a uniaxial nematic liquid crystal, the anisotropy of nematic phase is characterized by a symmetric and traceless tensor order parameter $Q_{\alpha\beta}$ which can be written as

$$Q_{\alpha\beta} = S(n_\alpha n_\beta - \frac{1}{3}\delta_{\alpha\beta}). \tag{8.1}$$

Here $n_\alpha$ and $n_\beta$ are components of the director $\mathbf{n}$, which is a unit vector with the property $\mathbf{n} = -\mathbf{n}$, describing the direction along which the molecules are aligned. And $S$ is the scalar order parameter that describes the degree of nematic order. It also represents how well the molecules are aligned along $\mathbf{n}$. If $S$ equal to 0, there is no alignment, which means that the system is in an isotropic phase; If $S$ equal to 1, it corresponds to a perfect alignment. When the director field $\mathbf{n}(\mathbf{r})$ changes drastically due to the distortion from undeformed ground state in nematic liquid crystal, it costs elastic energy for the deviation of the director, which can be classified into three types, namely splay, twist and bend, making the Frank-Oseen free energy density for elastic distortions reads as [47]

$$f_{el} = \frac{1}{2}K_{11}(\nabla \cdot \mathbf{n})^2 + \frac{1}{2}K_{22}[\mathbf{n} \cdot (\nabla \times \mathbf{n})]^2 + \frac{1}{2}K_{33}[\mathbf{n} \times (\nabla \times \mathbf{n})]^2, \tag{8.2}$$

where $K_{11}$, $K_{22}$ and $K_{33}$ are Frank elastic constants corresponding to splay, twist and bend constants, respectively. The bulk free energy of the nematic liquid crystal sample can be obtained by integrating $f_{el}$ over the sample volume

$$F_{el} = \int f_{el} dV. \tag{8.3}$$

LC molecules are sensitive to weak external stimuli, such as electric field, magnetic field and light, due to the anisotropic property of NLC. The facile response to weak external stimuli results in the easy distortion of director field when a magnetic or an electric field is applied. If an external magnetic filed is applied to the NLC, the following extra term should be added to the free energy

$$f_H = -\frac{1}{2}\Delta\chi(\mathbf{H}\cdot\mathbf{n})^2, \tag{8.4}$$

where $\mathbf{H}$ is the magnetic field and $\Delta\chi = \chi_\parallel - \chi_\perp$ is the diamagnetic anisotropy of the NLC, which can be positive or negative. Here $\chi_\parallel$ and $\chi_\perp$ are the two components of magnetic susceptibility for liquid crystal molecules when the magnetic field is applied. If $\Delta\chi > 0$, the molecules tend to align parallel to the direction of $\mathbf{H}$, while if $\Delta\chi < 0$, the molecules tend to align perpendicularly to the field direction. Analogously, if the external field is an electric one, then alternatively the additional free energy becomes

$$f_E = -\frac{1}{8\pi}\Delta\varepsilon(\mathbf{E}\cdot\mathbf{n})^2, \tag{8.5}$$

where $\mathbf{E}$ is the electric field and $\Delta\varepsilon = \varepsilon_\parallel - \varepsilon_\perp$ is the dielectric anisotropy of the NLC, which can be positive or negative as well. Here $\varepsilon_\parallel$ and $\varepsilon_\perp$ are the dielectric susceptibilities of the liquid crystal molecule parallel and perpendicular to the molecular long axis respectively. To illustrate how external fields alter the interactions of liquid crystal molecules, let us consider an NLC with thickness $L$ sandwiched between two cell walls, and we choose the coordinate $z$ axis normal to the cell walls where LC molecules are parallel to the $x$ direction, as depicted in Fig. 8.1. Suppose a magnetic field $\mathbf{H}$ is applied along the $z$ direction. Then the director field deviating from the undeformed director $\mathbf{n}_0 = (0,0,1)$ is given by

$$\mathbf{n}(z) = (\cos\theta(z), 0, \sin\theta(z)), \tag{8.6}$$

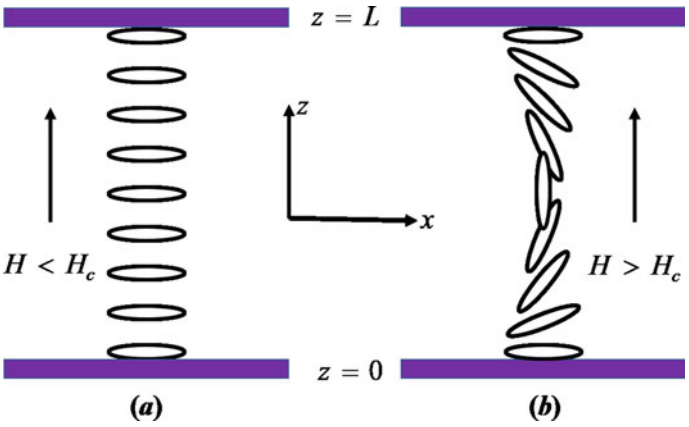


**Fig. 8.1** Sketch of Fréedericksz transition. The director $\mathbf{n}$ is fixed in the $x$ direction at the two plates of the cell, while the direction of the applied magnetic field $H$ is perpendicular to the cell walls. **a** If $H$ is below a certain critical field $H_c$, the NLC remains aligned in the $x$ direction. **b** If $H$ is above $H_c$, the NLC molecules start to try to realign along the $z$ direction

where $\theta$ is the angle between the director and $z$ axis, satisfying the boundary condition $\theta(0) = \theta(L) = 0$ due to the surface anchoring. The total free energy is then

$$F_{total} = \frac{1}{2}\int dz \left[ (K_{11}\cos^2\theta(z) + K_{33}\sin^2\theta(z))(\frac{d\theta(z)}{dz})^2 - \Delta\chi H^2 \sin^2\theta(z) \right]. \tag{8.7}$$

To obtain the distribution $\theta(z)$ corresponding to minimum total free energy, we calculate the functional derivative of the total free energy with respect to $\theta(z)$. Using one Frank constant approximation $K_{11} = K_{33} = K$ leads to the Euler-Lagrange equation

$$\frac{d^2\theta(z)}{dz^2}) + \frac{1}{\xi^2}\sin\theta(z)\cos\theta(z) = 0, \tag{8.8}$$

where $\xi = \sqrt{K/(\Delta\chi H^2)}$ is called the magnetic coherence length. When the magnetic field is small (i.e., $L/\xi$ is small), the solution is $\theta(z) = 0$. However, the solutions vary as the magnetic field increases and exceeds a certain threshold. To address this problem, we assume the functional form of $\theta(z)$ can be approximated by

$$\theta(z) = \theta_0 \sin(\frac{\pi z}{L}). \tag{8.9}$$

If $\theta_0 \ll 1$, substituting Eq. (8.9) into the total free energy of Eq. (8.7) and integrate over $z = 0$ to $L$, we obtain

$$F_{total} = \frac{\pi^2 K}{4L}\theta_0^2 - \frac{\Delta\chi L H^2}{4}\theta_0^2 = \frac{\Delta\chi L}{4}(H_c^2 - H^2)\theta_0^2, \tag{8.10}$$

where $H_c$ is the critical field

$$H_c = \frac{\pi}{L}\sqrt{\frac{K}{\Delta\chi}}. \tag{8.11}$$

Below the critical field (i.e., $H < H_c$), we have the solution $\theta_z = 0$ throughout the cell, and the NLC remains aligned in the $x$ direction (see Fig. 8.1a). If $H > H_c$ the deviation of the director field takes place (see Fig. 8.1b) and such a order transition called the Fréedericksz transition.

When a microparticle is introduced into the NLC, the microparticle interacts with the surrounding liquid crystal primarily via surface anchoring. The resulting surface anchoring free energy can be expressed as an integral over the microparticle surface in the Rapini-Popular form [1, 48]

$$F_{anchoring} = \frac{1}{2}W\int (\mathbf{n}\cdot\nu)^2 \mathbf{dS} \tag{8.12}$$

where $W$ is the anchoring coefficient and $\nu$ is a unit vector along the easy axis. Typically, the order of magnitude of $W$ varies within the range $10^{-4}$ mJ/m$^2$ − 1 mJ/m$^2$,

where $10^{-3} - 10^{-4}$ mJ/m$^2$ is considered as weak anchoring and $1 - 10^{-1}$ mJ/m$^2$ is regard as strong anchoring. In most cases the inclusion of particles into an NLC cell tends to create LC alignment singularities around the suspended substances, which in general are determined by surface anchoring conditions, particle size, boundary conditions, and external fields etc. [17, 49–52]. It has been widely accepted and confirmed that when a spherical particle is immersed in NLC, there are three possible types of defect configurations [53–55]. Dipole and quadrupolar configurations are usually seen around a spherical particle with strong vertical surface anchoring, whereas boojum defect is formed by a micro-sphere with tangential surface anchoring. In addition, recently B. Senyuk et al. assumed that conically degenerate boundary condition gives rise to the so-called elastic hexadecapole [56], and then Y. Zhou reported that the dipole-hexadecapole transformation can be achieved via tuning the preferred tilt angle of LC molecules anchoring on colloidal particle surface [57]. Through experimental observations it has been found that, when an external field is applied, there exists a transition between elastic dipole and quadrupolar configuration, which depends on particle size and surface anchoring strength [58–60].

As an application of the above theory, let us first of all consider a system that a particle is embedded in a uniform NLC without confinement. There are now two contributions to the free energy. The first contribution is the elastic deformation of the LC and can be accounted by the well known Frank-Oseen free energy. With one constant approximation $K_{11} = K_{22} = K_{33} = K$, the bulk deformation energy can be written as

$$F_b = \frac{K}{2} \int dV[(\nabla \cdot \mathbf{n})^2 + (\nabla \times \mathbf{n})^2]. \tag{8.13}$$

The second contribution is the surface anchoring free energy which is in the Rapini-Popula form Eq. (8.12), and the integration is over the particle surface. To determine the distribution of the director field $\mathbf{n}(\mathbf{r})$ for a particle embedded in a NLC, the goal is solve the Euler-Lagrange equations arising from the variation of the total free energy $F = F_b + F_{anchoring}$. Unfortunately, the Euler-Lagrange equations with subjected boundary conditions at the surface of the particle and parallel boundary conditions at infinity are highly nonlinear, and analytical solutions are quite difficult to found. However, utilising the multipole expansion method similar to electrostatic [61], we can obtain analytic solutions for the director field far from the particle. We assume that the director field at infinite approach the undeformed director field $\mathbf{n}_0$ = (0,0,1) when there is no other confinement. The deviation of $\mathbf{n}(\mathbf{r})$ from $\mathbf{n}_0$ induced by the embedded particle is small at the large distance but not infinite, and $\mathbf{n}(\mathbf{r}) \approx (\mathbf{n}_x, \mathbf{n}_y, 1)$. Therefore, at large $r$, the nonlinear bulk free energy of deformation can be replaced by the harmonic free energy [53, 55]

$$F_{har} = \frac{K}{2} \int dV (\nabla n_\mu)^2 \tag{8.14}$$

with Euler-Lagrange equations of Laplace type

$$\nabla^2 n_\mu = 0. \tag{8.15}$$

Here $n_\mu$ ($\mu = x, y$) represents the components of the director field $\mathbf{n}$ perpendicular to $\mathbf{n}_0$. Expanding the solutions into multipoles and we have the form of the solutions as follows [53, 55]

$$n_x = p\frac{x}{r^3} + 3c\frac{xz}{r^5}, \tag{8.16}$$

$$n_y = p\frac{y}{r^3} + 3c\frac{yz}{r^5}, \tag{8.17}$$

where $p$ and $c$ are the magnitude of the dipole and quadrupole moments respectively. If a particle is immersed in a NLC with confinement (i.e., NLC cell) and in the presence of external electric field, another surface anchoring free energy at the two plates of the cell and free energy arising from the applied electric field are need to be added. Thus our task is to minimize the more complicated total free energy functional. Unfortunately, it becomes more difficult to find the analytical solutions for the system of a particle suspended in a NLC cell in the presence of external field. Therefore, it is necessary to develop a phenomenological method to address this problem [40, 55], and this approach is introduced in the next section.

## 8.3 Theoretical Modeling

In order to introduce the phenomenological method mentioned above in details, we take the system that a spherical microparticle of radius $r$ suspended in a NLC cell sandwiched between two parallel plates a distance $L$ apart in the presence of an electric field as an example. The polarization of the particle is neglected compared with the influence of external field on the alignment of liquid crystal molecules. Figure 8.2 illustrates two systems schematically under external field with a homeotropic anchoring (Fig. 8.2a) and a homogeneous planar anchoring (Fig. 8.2b) respectively at the two cell walls. The suspended microparticle induces the director distortion and the director deviations $n_\mu$ ($\mu = x, y$) from the undeformed director field $\mathbf{n}_0 = (0,0,1)$ are small at the region far from the microparticle. In order to use the same set of symbol subscripts ($n_\mu$ ($\mu = x, y$)) in our theoretical modelling for the two surface anchoring conditions, two different coordinate frames are deliberately used here, as illustrated in Fig. 8.2a and b. Assuming $\mathbf{n} \approx (n_x, n_y, 1)$ with one Frank constant approximation, the effective elastic energy for the system reads [42]

$$U_e = K\int d^3x\Big[\frac{(\nabla n_\mu)^2}{2} - \frac{k^2}{2}(\mathbf{e}\cdot\mathbf{n})^2 - 4\pi P(\mathbf{x})\partial_\mu n_\mu - 4\pi C(\mathbf{x})\partial_z\partial_\mu n_\mu\Big], \tag{8.18}$$

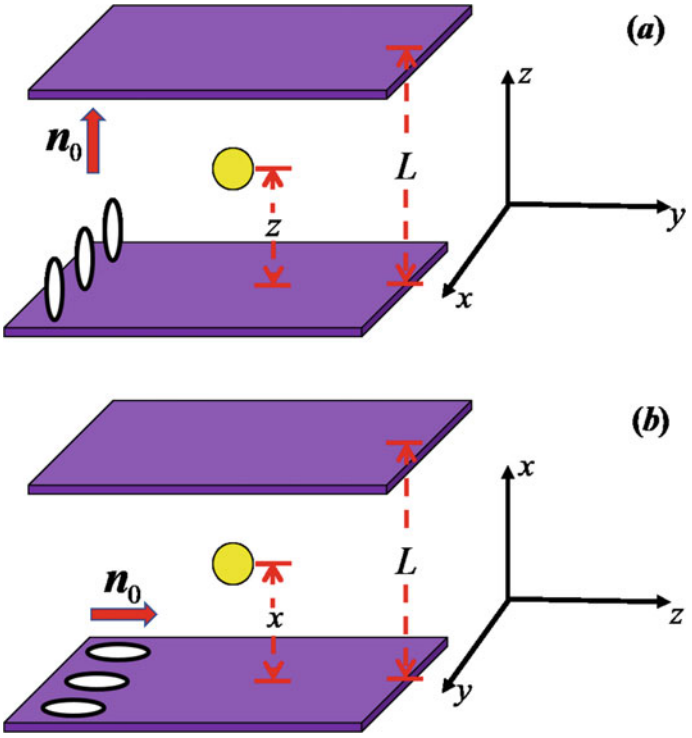


**Fig. 8.2** Schematic representation of a microparticle of radius $r$ suspended in a nematic liquid crystal cell with surface-to-surface distance $L$ and **a** normal anchoring and **b** planar anchoring in the presence of an external electric field

where $k^2 = (4\pi K)^{-1}\Delta\varepsilon E^2$, $P(\mathbf{x})$ and $C(\mathbf{x})$ denote the dipole and the quadrupole moment densities respectively. When an electric field is applied along $z$ axis, the Euler-Lagrange equation are given by [42]

$$\Delta n_\mu - k^2 n_\mu = 4\pi[\partial_\mu P(\mathbf{x}) - \partial_z \partial_\mu C(\mathbf{x})]. \tag{8.19}$$

When the external electric field is applied parallel to $x$ axis, we have the Euler-Lagrange equations written as [42]

$$\Delta n_\mu + k^2 \delta_{x\mu} n_\mu = 4\pi[\partial_\mu P(\mathbf{x}) - \partial_z \partial_\mu C(\mathbf{x})]. \tag{8.20}$$

If the applied electric field is parallel to $y$ axis, then the Euler-Lagrange equations are [42]

$$\Delta n_\mu + k^2 \delta_{y\mu} n_\mu = 4\pi[\partial_\mu P(\mathbf{x}) - \partial_z \partial_\mu C(\mathbf{x})]. \tag{8.21}$$

With Dirichlet boundary conditions $n_\mu(\mathbf{s}) = 0$ on the two walls, the solution to Euler-Lagrange equations can be written as [42]

$$n_\mu(\mathbf{x}) = \int_V d^3\mathbf{x}' G_\mu(\mathbf{x}, \mathbf{x}')[-\partial'_\mu P(\mathbf{x}') + \partial'_\mu \partial'_z C(\mathbf{x}')], \tag{8.22}$$

where $G_\mu$ is the Green's function for $n_\mu$. Notice that here $\mu$ in the integral does not follow Einstein summation notation.

## 8.4 Results and Discussions

### *8.4.1 Homeotropic Boundary Condition*

#### 8.4.1.1 External Field Perpendicular to the Two Plates

Here we choose the coordinate $z$ axis along the normal direction of the two cell walls where LC molecules are homeotropically anchored, as depicted in Fig. 8.2a). In the first case, when an electric is applied perpendicular to the two plates, i.e., $\mathbf{E} \| z$ in Fig. 8.2a, the corresponding Euler-Lagrange equations are written as Eq. (8.19). With Dirichlet boundary conditions $n_\mu(z = 0) = n_\mu(z = L) = 0$, the Green's function can be derived as [42]

$$G_\mu(\mathbf{x}, \mathbf{x}') = \frac{4}{L} \sum_{n=1}^{\infty} \sum_{m=-\infty}^{\infty} e^{im(\varphi - \varphi')} \sin \frac{n\pi z}{L} \sin \frac{n\pi z'}{L} I_m(\lambda_n \rho_<) K_m(\lambda_n \rho_>). \tag{8.23}$$

Here $\varphi$ and $\varphi'$ are the azimuthal angles, $z$ and $z'$ are the positional coordinates, $I_m$ and $K_m$ are modified Bessel functions, $\rho_<$ is the smaller one between $\sqrt{x^2 + y^2}$ and $\sqrt{x'^2 + y'^2}$, and $\lambda_n = [(n\pi/L)^2 + \Delta\varepsilon E^2/4\pi K]^{1/2}$ with $L$ the thickness of the NLC cell. Using the definition of self energy given in terms of Green's function[42]

$$U_{dd}^{self} = -2\pi K p^2 \partial_\mu \partial'_\mu H_\mu(\mathbf{x}, \mathbf{x}')|_{\mathbf{x}=\mathbf{x}'}, \tag{8.24}$$

where $H_\mu(\mathbf{x}, \mathbf{x}') = G_\mu(\mathbf{x}, \mathbf{x}') - 1/|\mathbf{x} - \mathbf{x}'|$, we can obtain the elastic energy $U_e^I$ for an NLC cell with a microparticle suspended in the presence of an electric field. Besides the elastic energy, the gravitational potential $U_g$ due to buoyant force should be considered as well, leading to a total energy written as

$$\begin{aligned} U_{total}^I &= U_e^I + U_g \\ &= -2\pi K p^2 \left[ -\frac{4}{L} \sum_{n=1}^{\infty} \lambda_n^2 \sin^2\left(\frac{n\pi z}{L}\right) K_0(\lambda_n \rho) + \frac{1}{\rho^3} \right]_{\rho \to 0} - \frac{4}{3}\pi r^3 (\rho_{LC} - \rho_{mp}) g z, \end{aligned} \tag{8.25}$$

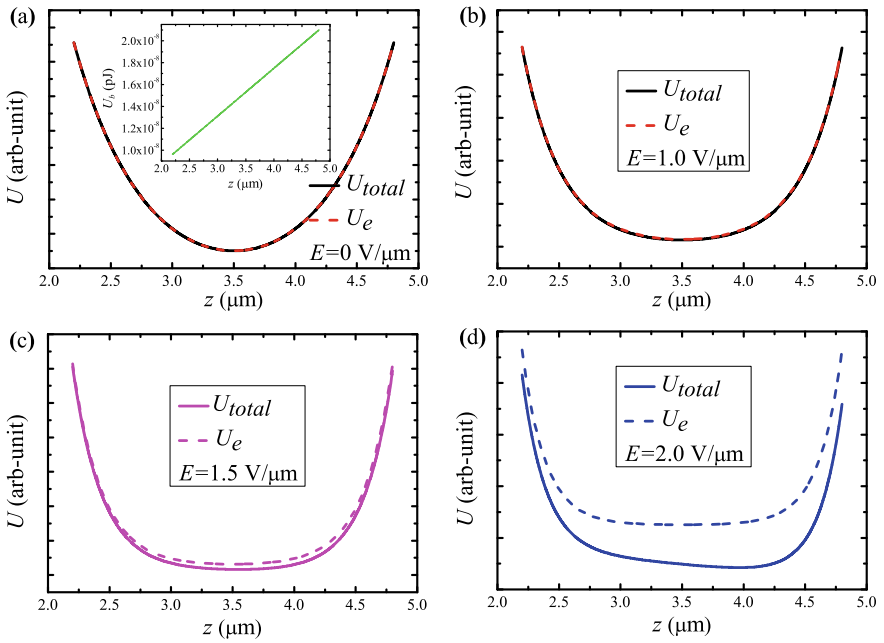


**Fig. 8.3** Elastic energy and total energy as a function of microparticle position for different electric fields (0, 1.0, 1.5 and 2.0 $V/\mu$m). Here we set the radius of microparticle and cell thickness as 2.2 $\mu$m and 7 $\mu$m, respectively

where $r$ is the radius of microparticle, $p = 2.04r^2$ is the magnitude of the equivalent dipole moment, $\rho_{LC} - \rho_{mp}$ is the density difference between liquid crystal and microparticle, $g = 9.8$ m/s$^2$ is the gravitational acceleration, and $z$ denotes the position of microparticle.

Based on the total energy obtained by Green's function method, we now plot the profiles of total energy as a function of microparticle position for different electric field. Let us first consider the case $\Delta\varepsilon > 0$. The total energy and elastic energy against for four different electric field strengths are shown in Fig. 8.3. In the presence of a small external electric field, the total energy given by Eq. 8.25 overlaps the elastic energy $U_e^I$ and remains symmetric, indicating that the interaction among LC molecules still dominates the system if the external field applied is not large enough to realign the LC molecules, especially in the region close to the midplane. Thus the contribution made by asymmetric gravitational potential is trivial and the microparticle in this case is still trapped within its midplane, as shown in Fig. 8.3b and c. However, as we increase the field applied, it tends to widen and flatten the bottom of the elastic potential well and that by contrast enlarges the relative contribution made by the asymmetric buoyant force to the total energy. As a result, the buoyant force will drive the microparticle with ease from midplane to a new equilibrium position (Fig. 8.3d). It is obvious that the sign of $\rho_{LC} - \rho_{mp}$ determines the direction

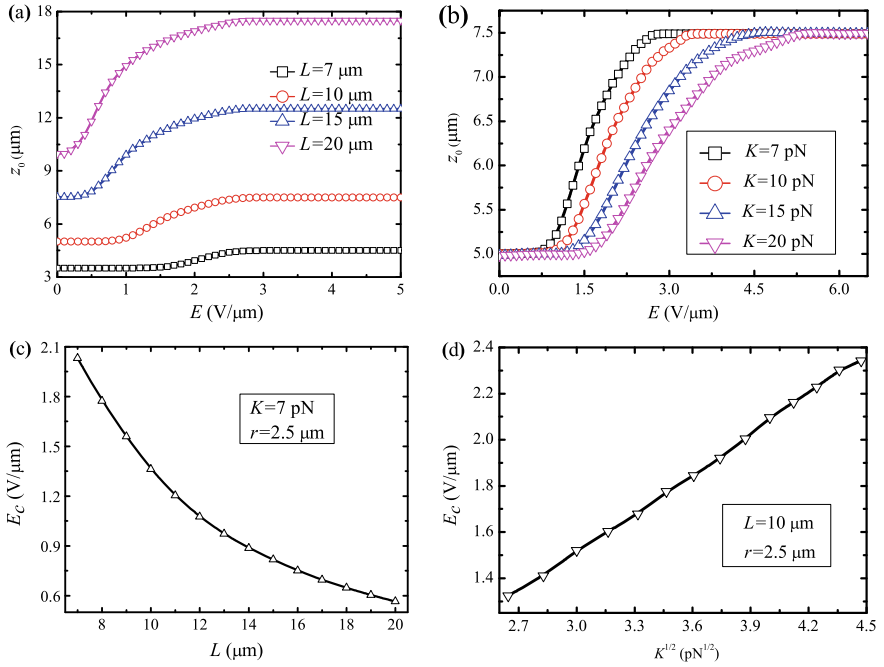


**Fig. 8.4** Equilibrium position $z_0$ in response to electric field for different **a** cell thicknesses (7, 10, 15 and 20 μm), where the Frank elastic constant and the radius of microparticle are set as $K = 7$ pN and $r = 2.5$ μm respectively, and **b** Frank elastic constants (7, 10, 15 and 20 pN), where the cell thickness and the radius of microparticle are set as $L = 10$ μm and $r = 2.5$ μm respectively. These two figures show a positional transition occurring at an electric field threshold $E_c$, which depends on **c** cell thickness $L$ and **d** Frank elastic constant $\sqrt{K}$

of particle displacement with respect to the original equilibrium position. It seems that the interaction potential well around the midplane tends to be flattened due to the realignment of liquid crystal molecules made by the applied external field, which creates a "fast lane" in the vertical direction for the microparticle to move. It triggers a positional transition from the midplane, if driven by an asymmetric buoyant force, when such a fast lane is fast enough (weakens the elastic energy gradient).

Furthermore, in order to study the effect of the cell thickness and Frank constant on the critical electric value, we plot the equilibrium position against the applied electric field for different cell thicknesses (7, 10, 15 and 20 μm) and Frank elastic constants (7, 10, 15 and 20 pN), as shown in Fig. 8.4a and b. It is found that a positional transition occurs when the external field applied exceeds a threshold value. The thinner the cell thickness $L$ is and the larger the Frank elastic constant $K$ is, the larger the critical electric field is needed to trigger the transition, as shown in Fig. 8.4c and d. A deeper investigation shows that the critical value of electric field is inversely proportional to $L$ and linearly proportional to $\sqrt{K}$, a Fréedericksz-like behavior.

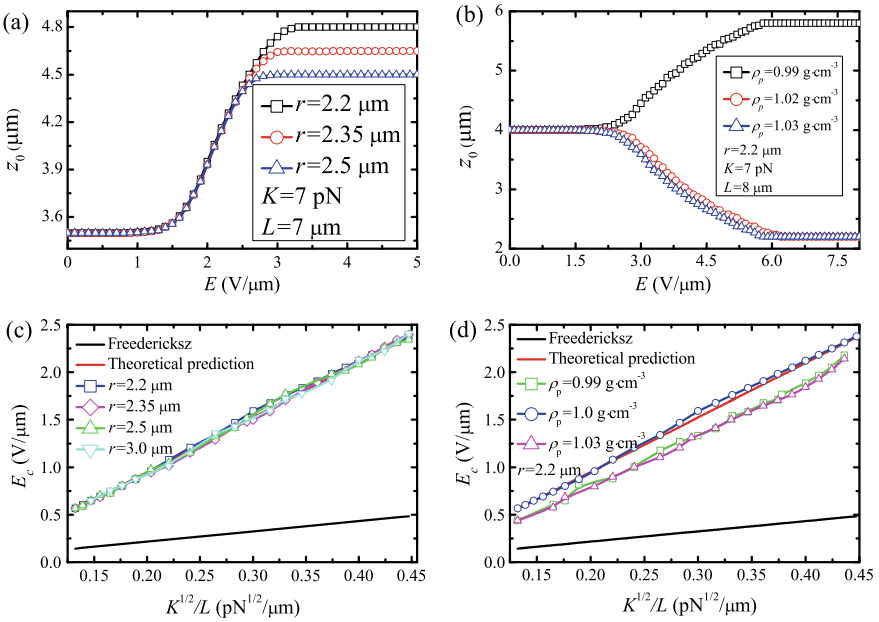


**Fig. 8.5** Equilibrium position $z_0$ for different **a** radii (2.2 μm, 2.35 μm and 2.5 μm) with $K = 7$ pN and $L = 7$ μm; **b** densities (0.99, 1.02 and 1.03 g · cm$^{-3}$) of microparticle with $K = 7$ pN and $L = 8$ μm, showing the same critical value $E_c$ of electric field triggering positional transition. The dependence of $E_c$ and $\sqrt{K}/L$ for different **c** radii (2.2 μm, 2.35 μm, 2.5 μm and 3.0 μm); **d** densities (0.99, 1.0 and 1.03 g · cm$^{-3}$) of microparticle, obeying strictly a master curve given by theoretical prediction Eq. (8.26)

In order to gain more insight into the dynamic behaviors of the microparticle, we investigate the dependence of threshold value on various microparticle's sizes and densities in Fig. 8.5. Figure 8.5a and b depict the equilibrium position against the applied electric field for different microparticle sizes and densities, where the overlapping of equilibrium position in Fig. 8.5a suggests that the critical electric value is almost independent of microparticle size. Whereas the symmetry of the equilibrium position of microparticle with density equal to 0.99 g · cm$^{-3}$ and 1.03 g · cm$^{-3}$ in Fig. 8.5b indicates that the slope of the master curve of critical electric value is nearly independent of the magnitude of microparticle density. Furthermore, to understand the dynamic behaviors of the microparticle, we plot the threshold value against $\sqrt{K}/L$ to obtain a master curve, as shown in Fig. 8.5c and d, where a Fréedericksz curve (black) is also plotted. It is interesting to find that the critical electric field to trigger a positional transition for microparticle suspended in a NLC cell follows a Fréedericksz-like linear master curve, yet with a different slope. The existence of slightly difference instead of overlapping to each other for the equilibrium position of microparticle with density equal to 1.02 g · cm$^{-3}$ and 1.03 g · cm$^{-3}$ in Fig. 8.5b, leads to different intercepts of the Fréedericksz-like linear master curves for critical

electric field in Fig. 8.5d. Obviously, the results indicate that the critical electric field for a positional transition to occur for a microparticle suspended in a NLC cell remains unchanged for different microparticle sizes and densities.

Moreover, by comparing the numerical calculation results with the Fréedericksz effect curve ($\pi\sqrt{4\pi/|\Delta\varepsilon|}\sqrt{K/L}$) in Fig. 8.5c and d, it is surprising to find that the slope difference between them is by a factor of $\sim 3\sqrt{\pi}$. The additional energy contribution coming from the surface energy due to the introduction of microparticle is proportional to $\pi$ (surface area). While on the other hand, the energy contribution made by external field is proportional to $E^2$, and that gives a critical value of external field proportional to $\sqrt{\pi}$, if the transition comes from the competition between equivalent surface energy due to the introduction of microparticle, and the Coulomb interaction due to the application of external field. More specifically, an explicit expression (where $\mathcal{F}$ denotes the Fréedericksz effect)

$$E_c \simeq 3\sqrt{\pi}\mathcal{F} - \frac{1}{5} = 6\pi^2\sqrt{\frac{K}{|\Delta\varepsilon|L^2}} - \frac{1}{5} \tag{8.26}$$

for critical electric field can be proposed as a theoretical prediction. Such a prediction, as shown by straight line (red) in Fig. 8.5c and d, agrees very well for different radii (2.2, 2.35, 2.5, and 3.0 μm) and densities (0.99, 1.0 and 1.03 g · cm$^{-3}$) of microparticle. This once again verifies the conclusion that the critical electric field is independent of microparticle size and density. The reason might lie in that in the present theoretical model, the microparticle is treated as a dipole in the far field expansion approximation.

In the case when $\Delta\varepsilon < 0$, the elastic energy and total energy as a function of microparticle position for two different electric field strengths is plotted as well, as shown in Fig. 8.6. Fig. 8.6a and b clearly show that the microparticle is trapped at

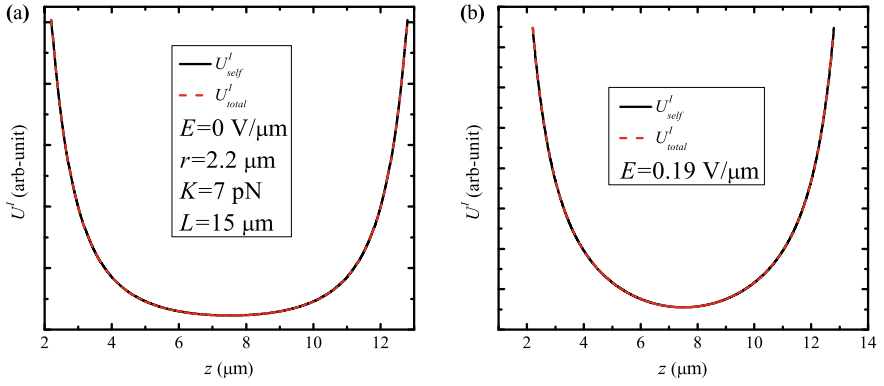


**Fig. 8.6** Elastic energy and total energy as a function of microparticle position for different electric fields **a** 0 $V/\mu$m and **b** 0.19 $V/\mu$m. Here the radius of microparticle, elastic constant and cell thickness are fixed at 2.2 μm, 7 pN and 15 μm, respectively

the midplane of the NLC cell, indicating that an application of external electric field does not trigger a positional phase transition. Moreover, in these two figures we also find that the electric filed has a crucial impact on the shape of potential well of elastic energy and total energy. This is because when $\mathbf{E}\|z$ and $\Delta\varepsilon < 0$, the realignment of liquid crystal molecules with the increase of the electric field narrows down the interaction potential well rather than flatten it (see Fig. 8.6), which creates a force directing toward the midplane much larger than the gravitational contribution and thus denies any positional transition.

#### 8.4.1.2 External Field Parallel to the Two Plates

For the case of an electric field parallel to the two plates, i.e., $\mathbf{E}\|x$ in Fig. 8.2a, the Euler-Lagrange equations for $n_x$ and $n_y$ are written as Eq. (8.20). With Dirichlet boundary conditions $n_\mu(z=0) = n_\mu(z=L) = 0$, the related Green's functions $G_x$ and $G_y$ are given by

$$G_x(\mathbf{x}, \mathbf{x}') = \frac{4}{L}\sum_{n=1}^{\infty}\sum_{m=-\infty}^{\infty} e^{im(\varphi-\varphi')}\sin\frac{n\pi z}{L}\sin\frac{n\pi z'}{L} I_m(\nu_n\rho_<)K_m(\nu_n\rho_>),$$
$$G_y(\mathbf{x}, \mathbf{x}') = \frac{4}{L}\sum_{n=1}^{\infty}\sum_{m=-\infty}^{\infty} e^{im(\varphi-\varphi')}\sin\frac{n\pi z}{L}\sin\frac{n\pi z'}{L} I_m(\mu_n\rho_<)K_m(\mu_n\rho_>), \quad (8.27)$$

where $\nu_n = [(n\pi/L)^2 - \Delta\varepsilon E^2/4\pi K]^{1/2}$ and $\mu_n = n\pi/L$. In analogue to the previous case, we can obtain the elastic energy $U_e^{II}$ and thereby the total energy $U_{total}^{II}$ is written as

$$\begin{aligned} U_{total}^{II} &= U_e^{II} + U_g \\ &= -2\pi K p^2\left[-\frac{2}{L}\sum_{n=1}^{\infty}\sin^2\left(\frac{n\pi z}{L}\right)(\alpha_n+\beta_n) + \frac{1}{\rho^3}\right]_{\rho\to 0} - \frac{4}{3}\pi r^3(\rho_{LC}-\rho_{mp})gz, \end{aligned} \quad (8.28)$$

where $\alpha_n = \nu_n^2 K_0(\nu_n\rho) + \mu_n^2 K_0(\mu_n\rho)$, and $\beta_n = \nu_n^2 K_2(\nu_n\rho) - \mu_n^2 K_2(\mu_n\rho)$.

In order to seek for the effect of electric field on the equilibrium position of microparticle, plots for the elastic energy and total energy against the microparticle position for different electric fields are presented in Fig. 8.7. When $\Delta\varepsilon > 0$, the narrows down of the potential well of elastic energy and total energy with the increase of electric field in Fig. 8.7a indicates that the microparticle tends to be trapped in the midplane of the NLC cell. When $\Delta\varepsilon < 0$, the increases of electric field tends to deepen and narrows down (which can hardly tell) the potential well of elastic energy and total energy, as illustrated in Fig. 8.7b. Due to the deep potential well, the microparticle is trapped in the midplane of the NLC cell regardless of the sign of the molecular dielectric anisotropy, indicating that an application of external elec-

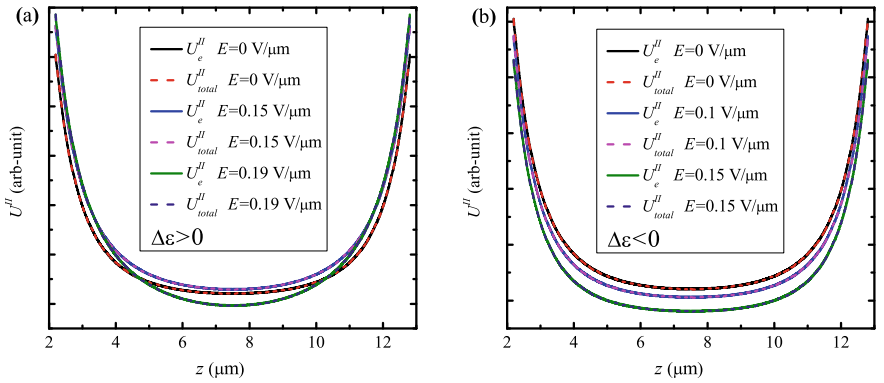


**Fig. 8.7** Elastic energy and total energy as a function of the microparticle position for different electric fields with **a** $\Delta\varepsilon > 0$ and **b** $\Delta\varepsilon < 0$. Here the radius of microparticle, elastic constant and cell thickness are fixed at 2.2 μm, 7 pN and 15 μm, respectively

tric field, however large it is, can not trigger a positional transition. This can be understood by considering the fact that the molecular long (short) axes tend to align along the direction of applied electric field as $\Delta\varepsilon > 0$ ($\Delta\varepsilon < 0$). As we increase the field applied, the interaction potential is found to be narrowed down and deepened, corresponding to a strong midplane-directing restoring force. Therefore for the homeotropic boundary condition, the positional transition occurs only in an NLC cell with positive molecular dielectric anisotropy when the external electric field is applied along the undeformed director field.

## *8.4.2 Planar Boundary Condition*

### 8.4.2.1 External Field Perpendicular to the Two Plates

Now we turn to the situation that LC molecules are horizontally anchored on the two cell walls and an electric field is applied vertically to the two plates, i.e., $\mathbf{E} \| x$, as depicted in Fig. 8.2b. The Euler-Lagrange equations are given by Eq. (8.20), and the corresponding Green's functions $G_x$ and $G_y$ read as [42]

$$G_x(\mathbf{x}, \mathbf{x}') = \frac{4}{L}\sum_{n=1}^{\infty}\sum_{m=-\infty}^{\infty} e^{im(\varphi-\varphi')} \sin\frac{n\pi x}{L} \sin\frac{n\pi x'}{L} I_m(\nu_n\rho_<)K_m(\nu_n\rho_>),$$
$$G_y(\mathbf{x}, \mathbf{x}') = \frac{4}{L}\sum_{n=1}^{\infty}\sum_{m=-\infty}^{\infty} e^{im(\varphi-\varphi')} \sin\frac{n\pi x}{L} \sin\frac{n\pi x'}{L} I_m(\mu_n\rho_<)K_m(\mu_n\rho_>), \quad (8.29)$$

with $\nu_n$ and $\mu_n$ identical to those in Eq. (8.27). Similarly, the elastic energy $U_e^{III}$ can be obtained and the total energy $U_{total}^{III}$ can be derived as

$$
\begin{aligned}
U_{total}^{III} &= U_e^{III} + U_g \\
&= -2\pi K p^2 \left[ \frac{4}{L} \sum_{n=1}^{\infty} \mu_n^2 \left[ \cos^2\left(\frac{n\pi x}{L}\right) K_0(\nu_n \rho) - \frac{1}{2} \sin^2\left(\frac{n\pi x}{L}\right) \left(K_0(\mu_n \rho) - K_2(\mu_n \rho)\right) \right] + \frac{1}{\rho^3} \right]_{\rho \to 0} \\
&\quad - \frac{4}{3}\pi r^3 (\rho_{LC} - \rho_{mp}) g x, \qquad (8.30)
\end{aligned}
$$

where $x$ denotes the vertical position of the microparticle.

In this case, let us first consider a positive dielectric anisotropy $\Delta\varepsilon > 0$. Intriguingly, a significant feature is observed regarding the profile of total energy as a function of microparticle position for four different electric fields, as illustrated in Fig. 8.8. In the presence of small field (below the critical electric value), Fig. 8.8a and b show that the interaction potential well around the midplane tends to be flattened in this region due to the realignment of liquid crystal molecules made by the increment of external electric field. However, when the electric field rises beyond the threshold value, there exists two symmetric equilibrium positions for the suspended microparticle (see Fig. 8.8c and d). Which one the microparticle shifts to is decided by the perturbation stemming from the asymmetric buoyant force, i.e. by the density difference between NLC and microparticle ($\rho_{LC} - \rho_{mp}$). Notably, the total energy now is almost equal to the elastic energy due to the fact that the gravitational

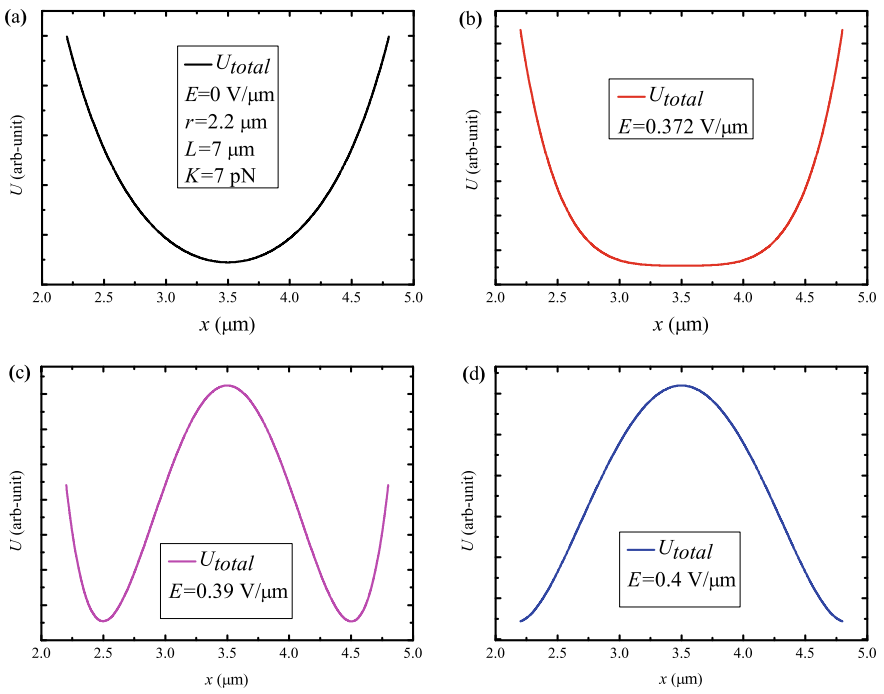


**Fig. 8.8** Total energy profile as a function of the suspended microparticle position for an NLC cell with planar anchoring in the presence of different electric fields perpendicular to the two plates

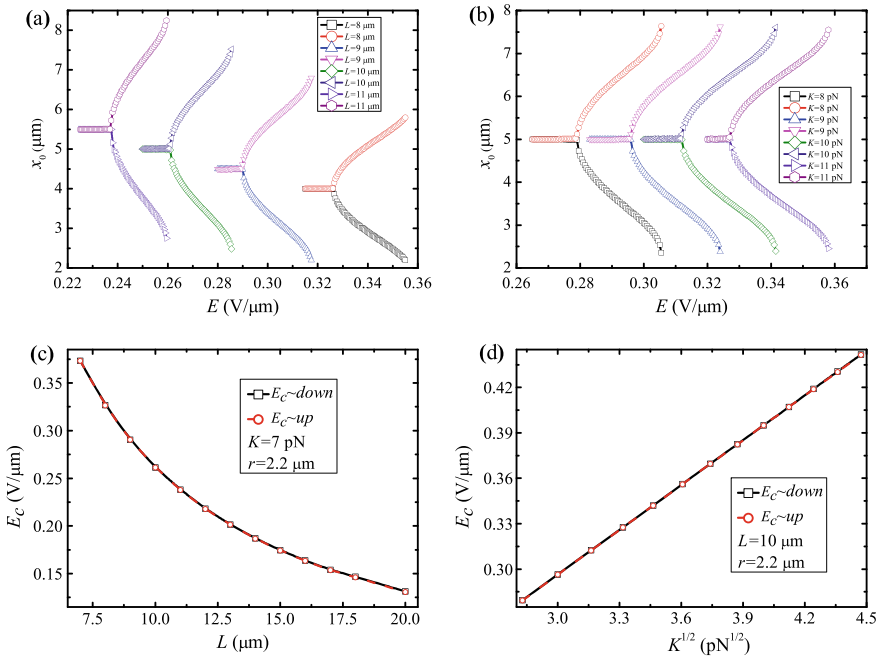


**Fig. 8.9** Equilibrium position $x_0$ in response to electric field for different **a** cell thicknesses (8, 9, 10 and 11 μm) with Frank elastic constant $K = 7$ pN and the radius of microparticle $r = 2.2$ μm, and **b** Frank elastic constants (8, 9, 10 and 11 pN) with cell thickness $L = 10$ μm and radius of microparticle $r = 2.2$ μm. It is shown that the electric field threshold $E_c$ at which a positional transition occurs, depends on **c** cell thickness $L$ and **d** Frank elastic constant $\sqrt{K}$

contribution is much smaller in contrast to the elastic one, generating the depths of the two local minimums in Fig. 8.8c (and Fig. 8.8d) nearly equal to each other.

To probe the influence of cell thickness and Frank constant on the critical field value, we plot the equilibrium position of the suspended microparticle against the applied electric field for different cell thicknesses (8, 9, 10 and 11 μm) and Frank elastic constants (8, 9, 10 and 11 pN), as shown in Fig. 8.9a and b, where a positional transition occurs at some electric field threshold values and there exist two bistable equilibrium positions when the external field applied exceeds the critical value. The thinner the cell thickness $L$ is and the larger the Frank elastic constant $K$ is, the larger the critical electric field is needed to trigger the positional transition, as shown in Fig. 8.9c and d. A more deeper investigation shows that the critical value of electric field is inversely proportional to $L$ and linearly proportional to $\sqrt{K}$, a Fréedericksz-like behavior.

As a following step, we examine whether the critical electric value is correlated with the size and density of the microparticle. Surprisingly, Fig. 8.10a and b show that the plots of the equilibrium position of suspended microparticle against the applied electric field for different microparticle sizes and densities overlap each other,

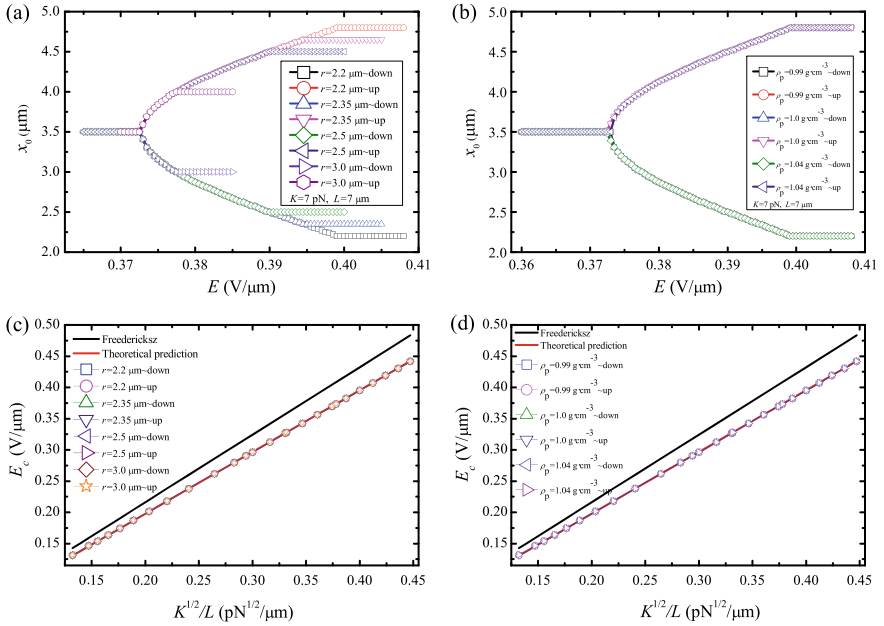


**Fig. 8.10** Equilibrium position $x_0$ for different **a** radii (2.2 μm, 2.35 μm, 2.5 μm and 3.0 μm); **b** densities (0.99, 1.0 and 1.04 g · cm$^{-3}$) of a microparticle with $K = 7$ pN and $L = 7$ μm, showing the same critical value $E_c$ of electric field triggering positional transition. The dependence of $E_c$ on $\sqrt{K}/L$ for different **c** radii (2.2 μm, 2.35 μm, 2.5 μm and 3.0 μm); **d** densities (0.99, 1.0 and 1.04 g · cm$^{-3}$) of the microparticle, obeying strictly a master curve which can be given by the theoretical prediction Eq. (8.31)

suggesting that the critical electric value is independent of or negligibly depends on microparticle size and density. To gain more insight into the dynamic behaviors of the microparticle, we further plot the threshold value against $\sqrt{K}/L$ in Fig. 8.10c and d, where a Fréedericksz curve (black) is shown as well. It is interesting to find that the critical electric field to trigger a positional transition for a microparticle suspended in an NLC cell follows a Fréedericksz-like linear master curve with slightly different slopes, a universal one also valid for different microparticle sizes and densities.

By comparing the numerical calculation results with the Fréedericksz transition ($\pi\sqrt{4\pi/|\Delta\varepsilon|}\sqrt{K}/L$) in Fig. 8.10c and d, we found that the slope difference between them is by a prefactor of ∼0.915, and that enables us to propose a theoretical prediction for the critical electric field

$$E_c \simeq 0.915\mathcal{F}, \tag{8.31}$$

where $\mathcal{F}$ denotes the Fréedericksz effect. Such a prediction, as shown by straight line (red) in Fig. 8.10c and d, agrees very well for different radii (2.2, 2.35, 2.5,

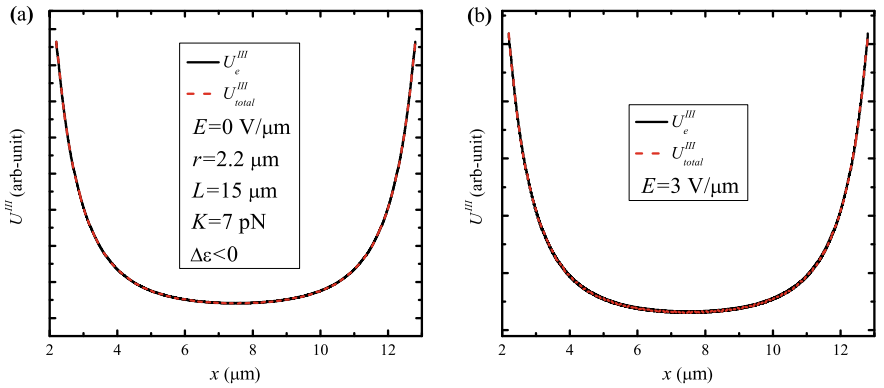


**Fig. 8.11** Elastic energy and total energy profile as a function of the suspended microparticle position for an NLC cell with planar anchoring in the presence of different electric fields perpendicular to the two plates. Here the radius of microparticle, elastic constant and cell thickness are set as 2.2 μm, 7 pN and 15 μm, respectively

and 3.0 μm) and densities (0.99, 1.0 and 1.04 g · cm$^{-3}$) of microparticle. Due to the mathematical difficulty, we still don't know how to derive 0.915 analytically.

In the case when $\Delta\varepsilon < 0$, to determine whether the positional transition phenomenons takes place or not, we plot the elastic energy and total energy against microparticle position for different electric field, as depicted in Fig. 8.11. The comparison of Fig. 8.11a and b shows that the potential well of elastic energy and total energy are narrowed down with the increase of electric field, indicating that the suspended microparticle is trapped at the midplane of the NLC cell, which can be predicted by the profile change of the total energy potential well due to application of an external electric field in the vertical direction ($x$ direction in Fig. 8.2b). The short axes of liquid crystal molecules tend to align along the electric field, a result leading to the narrowing of total potential well and thereby generating strong restoring force acting on the suspended microparticle. Therefore, in the case of a microparticle suspended in an NLC cell with planar anchoring condition in the presence of an external electric field applied perpendicular to the two plates, the positional transition triggered by the electric field occurs only under the condition of positive molecular dielectric anisotropy.

#### 8.4.2.2 External Field Parallel to the Two Plates but Perpendicular to the Anchoring Direction

Now let us consider the case when the electric field applied is parallel to the two plates but perpendicular to the anchoring direction, i.e., $\mathbf{E} \| y$ in Fig. 8.2b, the Euler-Lagrange equations can be given by Eq. (8.21), with their corresponding Green's functions $G_x$ and $G_y$ written as

$$G_x(\mathbf{x},\mathbf{x}') = \frac{4}{L}\sum_{n=1}^{\infty}\sum_{m=-\infty}^{\infty} e^{im(\varphi-\varphi')}\sin\frac{n\pi x}{L}\sin\frac{n\pi x'}{L} I_m(\mu_n\rho_<)K_m(\mu_n\rho_>),$$

$$G_y(\mathbf{x},\mathbf{x}') = \frac{4}{L}\sum_{n=1}^{\infty}\sum_{m=-\infty}^{\infty} e^{im(\varphi-\varphi')}\sin\frac{n\pi x}{L}\sin\frac{n\pi x'}{L} I_m(\nu_n\rho_<)K_m(\nu_n\rho_>), \quad (8.32)$$

with the same $\nu_n$ and $\mu_n$ as those in Eq. (8.29). In a similar way, the total energy $U_{total}^{IV}$ is given by

$$\begin{aligned} U_{total}^{IV} &= U_e^{IV} + U_g \\ &= -2\pi K p^2\left[\frac{4}{L}\sum_{n=1}^{\infty}\mu_n^2\cos^2(\frac{n\pi x}{L})K_0(\mu_n\rho) - \frac{2}{L}\sum_{n=1}^{\infty}\nu_n^2\sin^2(\frac{n\pi x}{L})\big(K_0(\nu_n\rho) - K_2(\nu_n\rho)\big) + \frac{1}{\rho^3}\right]_{\rho\to 0} \\ &\quad -\frac{4}{3}\pi r^3(\rho_{LC}-\rho_{mp})gx, \end{aligned} \quad (8.33)$$

where $U_e^{IV}$ is the elastic energy.

Similar to the previous cases, to probe the influence of electric field on the equilibrium position of microparticle, plots for the elastic energy and total energy against the microparticle position for different electric field are presented in Fig. 8.12. When $\Delta\varepsilon > 0$, the potential well of elastic energy and total energy in Fig. 8.12b are narrowed down as compared with that in Fig. 8.12a. When $\Delta\varepsilon < 0$, Fig. 8.12c and d show the same trend. Those results suggest that no matter $\Delta\varepsilon > 0$ or $\Delta\varepsilon < 0$, the microparticle is always trapped at the midplane of the NLC cell regardless of the magnitude of the electric field applied, indicating that no positional transition occurs. The reason lies in that the realignment of the liquid crystal molecules in the presence of the external electric field does not flatten the interaction potential well substantially enough so as to decrease its corresponding equivalent restoring force on the microparticle to a small magnitude, with which the asymmetric gravitational force becomes competitive.

#### 8.4.2.3 External Field Parallel to the Two Plates and the Anchoring Direction

Finally, we consider an NLC cell in the presence of an electric field parallel to the two plates and the anchoring direction as well, i.e., $\mathbf{E}\|z$ in Fig. 8.2b. Given the corresponding Euler-Lagrange equations Eq. (8.19), the Green's functions are [42]

$$G_\mu(\mathbf{x},\mathbf{x}') = \frac{4}{L}\sum_{n=1}^{\infty}\sum_{m=-\infty}^{\infty} e^{im(\varphi-\varphi')}\sin\frac{n\pi x}{L}\sin\frac{n\pi x'}{L} I_m(\lambda_n\rho_<)K_m(\lambda_n\rho_>), \quad (8.34)$$

with the same $\lambda_n$ as that in Eq. (8.23). Similarly, the total energy $U_{total}^{V}$ can be derived as

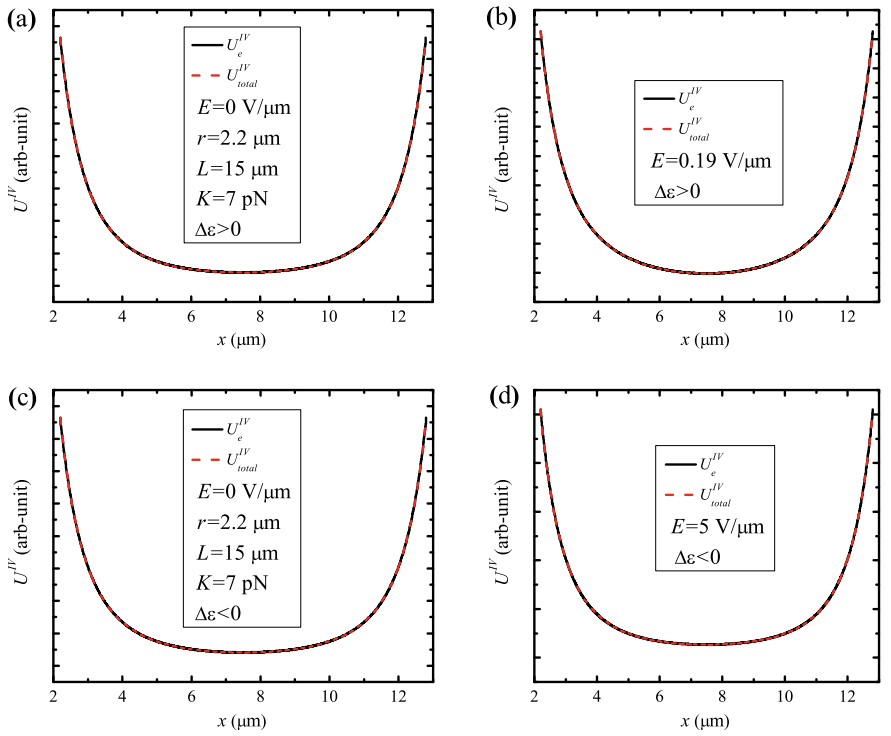


**Fig. 8.12** Elastic energy and total energy as a function of microparticle position for **a** $\Delta\varepsilon > 0$ and $E = 0\ V/\mu m$; **b** $\Delta\varepsilon > 0$ and $E = 0.19\ V/\mu m$; **c** $\Delta\varepsilon < 0$ and $E = 0\ V/\mu m$; **d** $\Delta\varepsilon < 0$ and $E = 5\ V/\mu m$;. Here the radius of microparticle, elastic constant and cell thickness are fixed at 2.2 μm, 7 pN and 15 μm, respectively

$$
\begin{aligned}
U_{total}^{V} &= U_e^{V} + U_g \\
&= -2\pi K p^2 \left[ \frac{4}{L} \sum_{n=1}^{\infty} \left(\frac{n\pi}{L}\right)^2 \cos^2\left(\frac{n\pi x}{L}\right) K_0(\lambda_n \rho) - \frac{2}{L} \sum_{n=1}^{\infty} \lambda_n^2 \sin^2\left(\frac{n\pi x}{L}\right) \left(K_0(\lambda_n \rho) - K_2(\lambda_n \rho)\right) + \frac{1}{\rho^3} \right]_{\rho \to 0} \\
&\quad - \frac{4}{3}\pi r^3 (\rho_{LC} - \rho_{mp}) g x,
\end{aligned}
\tag{8.35}
$$

with $U_e^V$ the elastic energy.

Given a positive molecular dielectric anisotropy, namely $\Delta\varepsilon > 0$, we can plot, as shown in Fig. 8.13, the total energy profile as a function of the suspended microparticle position for four chosen electric fields. In the presence of a small external field, the total energy profile remains symmetric, indicating that the elastic interaction among LC molecules dominates the LC alignment, especially in the region close to the midplane. Thus the contribution made by asymmetric gravitational potential is trivial if compared with elasticity and the suspended microparticle will be trapped within its midplane, as demonstrated in Fig. 8.13a and b. While as the electric field is increased, it is found that it tends to widen and flatten the bottom of the elastic poten-

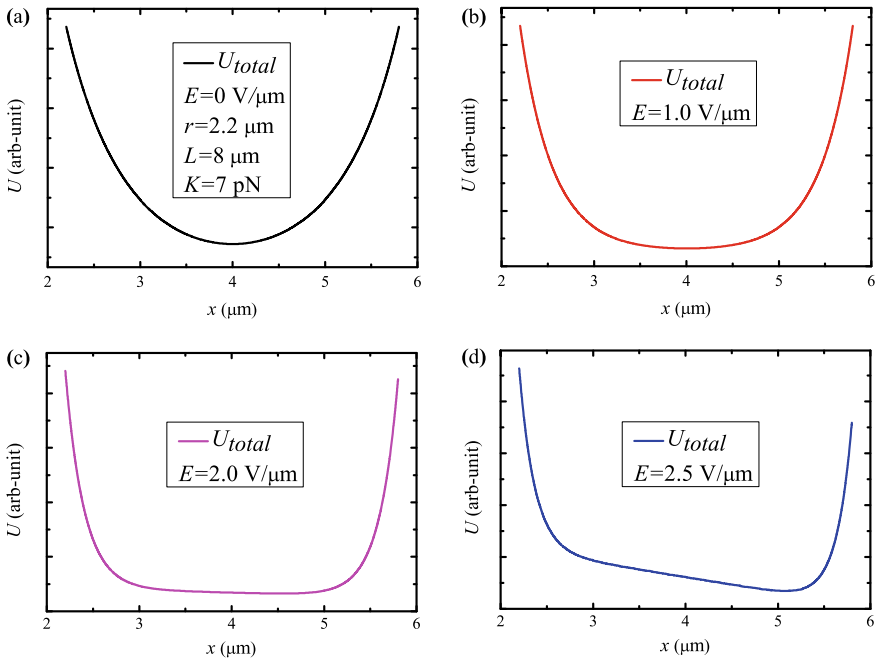


**Fig. 8.13** Total energy profile as a function of the suspended microparticle position for an NLC cell with planar anchoring in the presence of four chosen electric fields parallel to the two plates and the anchoring direction as well

tial well, which equivalently by contrast amplifies the relative contribution made by the asymmetric buoyant force to the total energy of the NLC cell. As a result, the buoyant force will drive the microparticle with ease from the midplane to a new equilibrium position (see Fig. 8.13c and d). It is apparent that the sign of $\rho_{LC} - \rho_{mp}$ determines the direction of the microparticle displacement. It looks very much like that the bottom of the interaction potential well around the midplane is "pressed due to the realignment of liquid crystal molecules made by the applied external field, which creates a "fast lane" along the vertical direction in the cell for the suspended microparticle to migrate. Once such a "fast lane" constructed by the external field in the cell reaches a critical value of "smoothness" (corresponding to a weakened elastic energy gradient), driven by the asymmetric buoyant force, it triggers a positional transition for the suspended microparticle from the midplane to its new equilibrium position.

In order to study the influence of cell thickness and Frank constant on the critical value of electric field, plots for the equilibrium position for the suspended microparticle against the applied electric field for different cell thicknesses (8, 10, 12 and 15 μm) and Frank elastic constants (8, 10, 12 and 15 pN) are presented in Fig. 8.14a and b, where it is found that a positional transition occurs when the external field applied exceeds a threshold value. It is also shown that the thinner the cell thickness

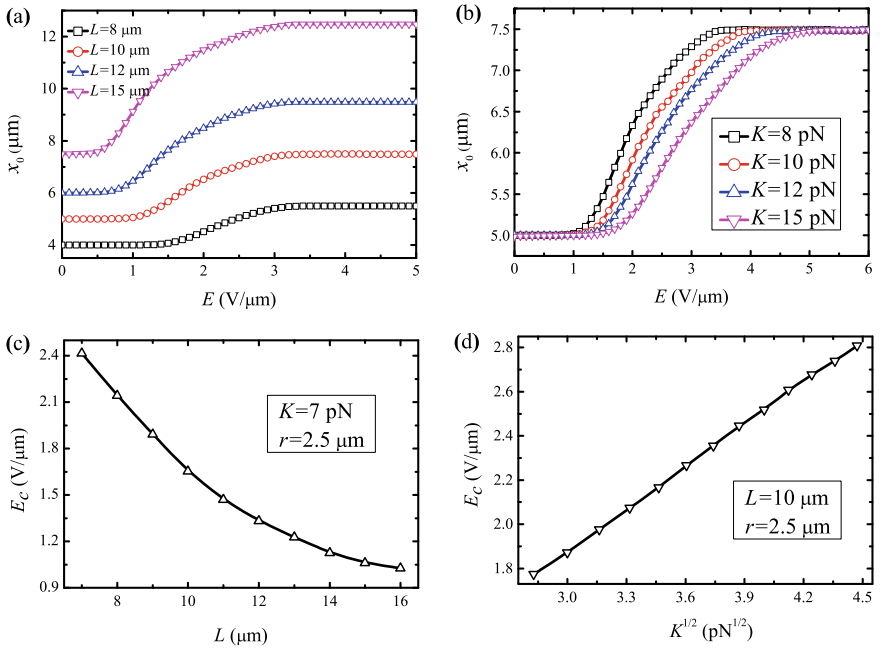


**Fig. 8.14** Equilibrium position $x_0$ in response to electric field for different **a** cell thicknesses (8, 10, 12 and 15 μm), where the Frank elastic constant and the radius of microparticle are set as $K = 7$ pN and $r = 2.5$ μm, and **b**Frank elastic constants (8, 10, 12 and 15 pN), where the cell thickness and the radius of microparticle are set as $L = 10$ μm and $r = 2.5$ μm. The electric field threshold $E_c$ depends on **c** cell thickness $L$ and **d** Frank elastic constant $\sqrt{K}$

$L$ is and the larger the Frank elastic constant $K$ is, the larger the critical electric field is needed to trigger the positional transition. The further study of electric field threshold (see Fig. 8.14c and d) shows that it seems to be inversely proportional to cell thickness $L$ and proportional to the root square of Frank elastic constant $K$, a behavior similar to the field threshold of Fréedericksz phase transition.

In a similar way to the previous sections, the dependence of the threshold value on microparticles size and density is also investigated. Figure 8.15a and b depict the equilibrium position against the applied electric field for different microparticle sizes and densities, where the overlapping of equilibrium position in Fig. 8.15a suggests that the critical electric value is almost independent of microparticle size. Whereas the symmetry of the equilibrium position of microparticle with density equal to 0.99 $g \cdot cm^{-3}$ and 1.03 $g \cdot cm^{-3}$ in Fig. 8.15b indicates that the slope of the master curve of critical electric value is nearly independent of the magnitude of equivalent microparticle density. To gain more insight into the dynamic behaviors of the microparticle, the threshold value is plotted against $\sqrt{K}/L$ in Fig. 8.15c and d, where a Fréedericksz transition curve (black) is shown as well. The existence of slightly difference instead of overlapping to each other for the equilibrium position

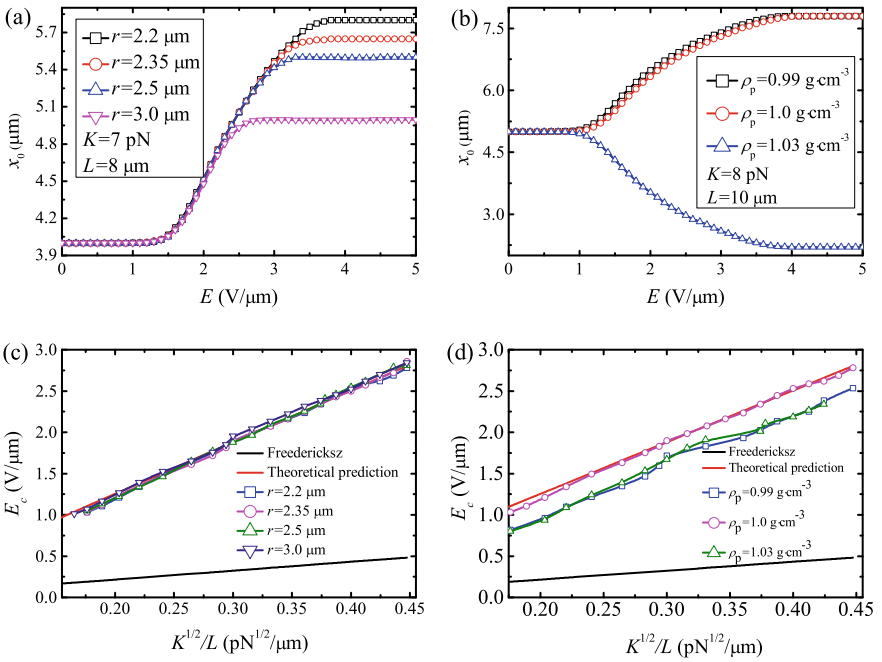


**Fig. 8.15** **a** Equilibrium position $x_0$ for different radii of microparticle with $K = 7$ pN and $L = 8$ μm, showing the same critical value $E_c$ of electric field triggering positional transition. **b** $K = 8$ pN and $L = 10$ μm. The dependence of $E_c$ and $\sqrt{K}/L$ for different **c** radii (2.2 μm, 2.35 μm, 2.5 μm and 3.0 μm); **d** densities (0.99, 1.0 and 1.03 g · cm$^{-3}$) of microparticle, obeying strictly a master curve given by theoretical prediction Eq. (8.36)

of microparticle with density equal to 0.99 g · cm$^{-3}$ and 1.0 g · cm$^{-3}$ in Fig. 8.15b, leads to different intercepts of the Fréedericksz-like linear master curves for critical electric field in Fig. 8.15d. Like before, the critical electric field for a positional transition to occur for a microparticle suspended in a NLC cell remains unchanged for different microparticle sizes and densities.

Similarly, a contrast between the numerical calculation results and the traditional Fréedericksz transition curve ($\pi\sqrt{4\pi/|\Delta\varepsilon|}\sqrt{K}/L$) in Fig. 8.15c and d shows that the slope difference between them is by a prefactor of $\sim 5.8$. More specifically, an explicit expression

$$E_c \simeq 5.8\mathcal{F} - 0.08 = 5.8\pi\sqrt{\frac{4\pi K}{|\Delta\varepsilon|L^2}} - 0.08 \tag{8.36}$$

for critical electric field can be proposed as a theoretical prediction. Such a prediction, as shown by straight line (red) in Fig. 8.15c and d, agrees very well for different radii (2.2, 2.35, 2.5, and 3.0 μm) and densities (0.99, 1.0 and 1.03 g · cm$^{-3}$) of microparticle. This once again verifies the conclusion that the critical electric field is

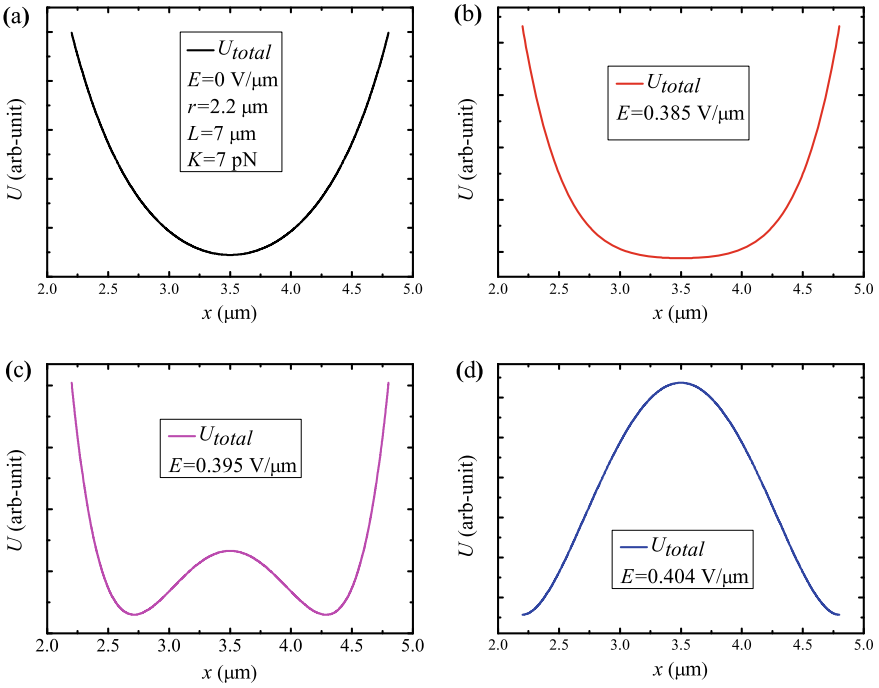


**Fig. 8.16** Total energy profile as a function of the suspended microparticle position for different external electric fields

independent of microparticle size, of which the reason might lie in that in the present theoretical model, the microparticle is approximately treated as a dipole in the far field expansion.

As for the case $\Delta\varepsilon < 0$ when the external field applied parallel to both the two plates and the anchoring direction, i.e., $\mathbf{E}\|z$ in Fig. 8.2b, a bistable equilibrium state structure is found as the electric field exceeds a threshold value, as illustrated in Fig. 8.16. In the small-field region, the external field applied tends to, first of all, flatten the bottom of potential well, as shown in Fig. 8.16a and b. Further increase of external field will change the one-state potential structure to a bistable one. As the gravitational contribution to the total energy is still negligibly small compared to the elastic one, one sees no involvement of gravitational force to the determination of the critical value of positional transition for the microparticle in the NLC cell. Thus, the positional transition in this case does not come from the competition between the gravitational force and the equivalent elastic force but rather purely from the bistable local minimum of the elastic potential, as shown in Fig. 8.16c and d. Nevertheless the asymmetric gravitational force still plays a very important role in determining the direction of microparticle motion (up or down) by acting as a small but significant

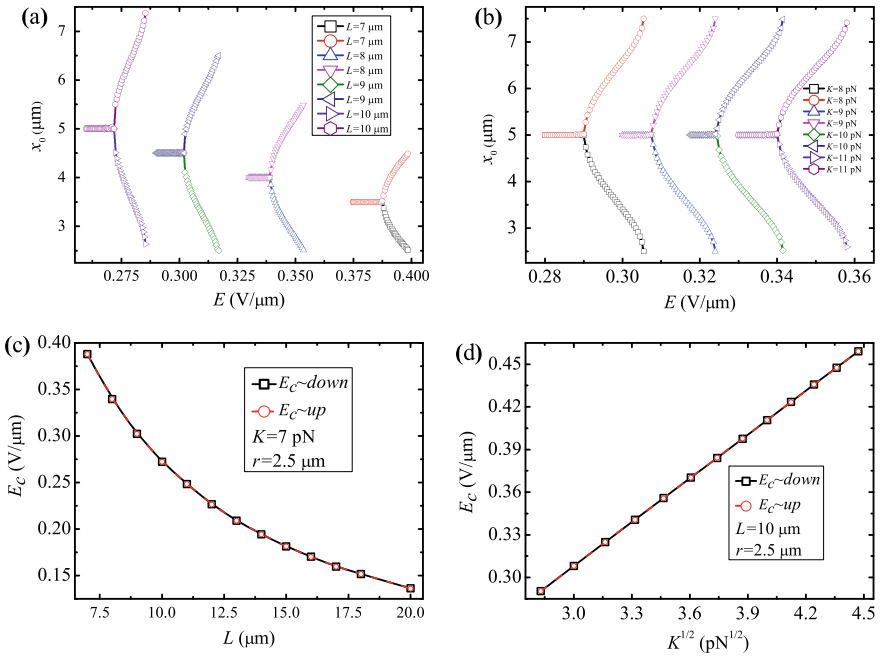


**Fig. 8.17** Equilibrium position $x_0$ in response to electric field for different **a** cell thicknesses (7, 8, 9 and 10 $\mu m$), where the Frank elastic constant and the radius of microparticle are set as $K = 7$ pN and $r = 2.5$ μm, and **b** Frank elastic constants (8, 9, 10 and 11 pN), where the cell thickness and the radius of microparticle are set as $L = 10$ μm and $r = 2.5$ μm. It is shown that a positional transition occurs at electric field threshold $E_c$, which depends on **c** cell thickness $L$ and **d** Frank elastic constant $\sqrt{K}$

perturbation, or more precisely, by the sign of buoyant force (the sign of $\rho_{LC} - \rho_{mp}$). Therefore, the magnitude of the asymmetric gravitational force in this case is trivial but not its sign.

In order to understand how cell thickness and Frank elastic constant affect the critical value of electric field, we plot equilibrium position against the applied electric field for different cell thicknesses (7, 8, 9 and 10 μm) and Frank elastic constants (8, 9, 10 and 11 pN), as shown in Fig. 8.17a and b, where a bifurcation of equilibrium position is found due to the bistable state structure of elastic potential and a positional transition occurs when the external field applied reaches a threshold value. Additionally, a Fréedericksz-like behavior is shown in Fig. 8.17c and d. As observed, the thinner the cell thickness $L$ is and the larger the Frank elastic constant $K$ is, the larger the critical electric field is needed to trigger the positional transition, which corresponding to that the critical value of electric field is inversely proportional to $L$ and linearly proportional to $\sqrt{K}$.

Finally, in order to gain more insights into the physics hidden behind the dynamic behaviors of microparticle, it is worthwhile to evaluate whether the critical electric

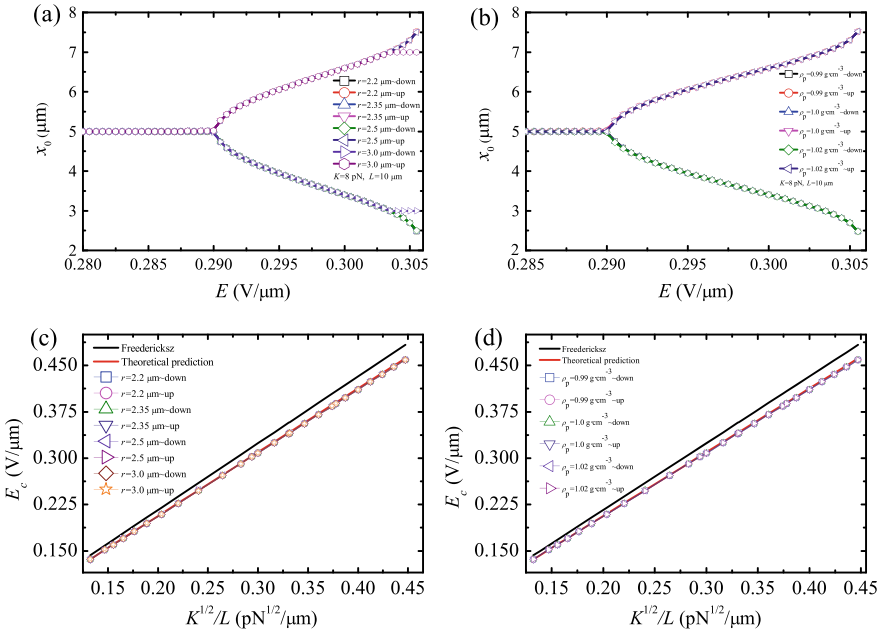


**Fig. 8.18** Equilibrium position $x_0$ for different **a** radii (2.2 μm, 2.35 μm, 2.5 μm and 3.0 μm); **b** densities (0.99, 1.0 and 1.02 g · cm$^{-3}$) of microparticle with $K = 8$ pN and $L = 10$ μm, showing the same critical value $E_c$ of electric field triggering positional transition. The dependence of $E_c$ and $\sqrt{K}/L$ for different **c** radii (2.2 μm, 2.35 μm, 2.5 μm and 3.0 μm); **d** densities (0.99, 1.0 and 1.02 g · cm$^{-3}$) of microparticle, obeying strictly a master curve given by theoretical prediction Eq. (8.37)

value is correlated with the size and density of the microparticle. The dependence of the equilibrium position on the applied electric field for different microparticle sizes and densities is shown in Fig. 8.18a and b, where the strict overlapping of equilibrium position in the figures implies that the critical electric value is, as shown in the previous section, independent of microparticle size and density. For a better understanding of the dynamic behaviors of the microparticle, we further plot the threshold value against $\sqrt{K}/L$ in Fig. 8.18c and d, with a Fréedericksz transition curve (black) shown as well. It is found that the critical electric field triggering a positional transition for a microparticle suspended in a NLC cell follows a Fréedericksz master curve irrelevant to microparticle size and density.

More precisely, by comparing the numerical calculation results with the Fréedericksz effect curve ($\pi\sqrt{4\pi/|\Delta\varepsilon|}\sqrt{K}/L$) in Fig. 8.18c and d, it is found that the slope difference between them is by a prefactor of $\sim 3/\pi$, leading to a proposed theoretical prediction for the critical electric field. Such a prediction, as shown by straight line (red) in Fig. 11c and d, agrees very well for different radii (2.2, 2.35, 2.5, and 3.0 μm) and densities (0.99, 1.0 and 1.02 g · cm$^{-3}$) of microparticle.

**Table 8.1** Formation of a vertical fast "lane" for positional transition to occur (+) and not to occur (−) for a microparticle suspended in an NLC cell in the presence of an external electric field

| Anchoring | Molecular dielectric anisotropy | Field direction | | |
|---|---|---|---|---|
| | | $\mathbf{E} \perp$ Plates | $\mathbf{E} \parallel$ Plates | |
| Homeotropic | $\Delta\varepsilon > 0$ | + | − | |
| | $\Delta\varepsilon < 0$ | − | − | |
| Planar | | | $\mathbf{E} \perp$ Anchoring | $\mathbf{E} \parallel$ Anchoring |
| | $\Delta\varepsilon > 0$ | +/bistable | − | + |
| | $\Delta\varepsilon < 0$ | − | − | +/bistable |

$$E_c \simeq \frac{3}{\pi}\mathcal{F} = 6\sqrt{\frac{\pi K}{|\Delta\varepsilon| L^2}} \tag{8.37}$$

Based on the discussions in the sections above, it is quite obvious that the external electric field applied enhances the existing anisotropy of distortion generated by the boundaries of the NLC cell shaped by the movable suspended microparticle and the two parallel walls. It looks like there exists an anisotropic movable "bubble" surrounding the suspended microparticle, created by the external field and the boundary conditions combined. Inside the "bubble" along the vertical direction a fast "lane" will be constructed once the external field applied reaches a critical value. The electric field threshold is a signal to complete the construction and a "key" to switching on the use of the fast "lane", wobbling the "bubble" along the vertical direction, and thereby tune the motion of the microparticle inside, which has been proved to be a positional transition [44]. Interestingly, this kind of motion can be found in the some SiFi novels picturing one of the possible tactics for intergalactic travel in the future by moving a planetary object via wobbling the space-time around it, which is supported by general relativity. After a thorough discussion of all the conditions combined to create such a wobbling "bubble" in a NLC cell in the presence of an external electric field, we come up with a table for a positional transition to occur in such a system, as shown in Table 8.1. It is found in the Table that out of the ten combinations of field direction, molecular dielectric anisotropy, and anchoring feature, only four shows the possible occurrence of positional transition. Moreover, for a nematic liquid crystal cell with planar surface alignment, a bistable equilibrium structure for the transition is found when the direction of applied electric field is (a) perpendicular to the two plates of the cell with positive molecular dielectric anisotropy, or (b) parallel to both the two plates and the anchoring direction of the cell with negative molecular dielectric anisotropy.

## 8.5 Conclusion

In summary, using the Green's function method, the total energy for a microparticle suspended in an NLC cell in the presence of an external electric field is calculated. It is found that with the application of the external electric field, it is possible to create an anisotropic bubble around the microparticle with a vertical fast "lane" for the microparticle to move from the midplane to a new equilibrium position. Such a new equilibrium position is decided via a competition between the buoyant force and the effective force built upon the microparticle inside the "lane". The threshold value of external field, which triggers positional transition under appropriate conditions of surface anchoring feature, field direction and molecular dielectric anisotropy, depends on thickness $L$ and Frank elastic constant $K$ and slightly on the microparticle size and density, in a Fréedericksz-like manner as coined by the authors before, but by a factor. For an NLC cell with planar surface alignment, a bistable equilibrium structure for the transition is found when the direction of the applied electric field is (a) perpendicular to the cell wall with positive molecular dielectric anisotropy, and (b) parallel to the undeformed director field $\mathbf{n}_0$ of the NLC cell with negative molecular dielectric anisotropy. When the electric field applied is parallel to the two plates and perpendicular to the anchoring direction, the microparticle suspended in NLC will be trapped in the midplane, regardless of the sign of the molecular dielectric anisotropy. Explicit formulae proposed for the critical electric field agrees extremely well with the numerical calculation.

## References

1. de Gennes, P.G., Prost, J.: The Physics of Liquid Crystals, 2nd edn. Clarendon Press, Oxford, UK (1993)
2. Jákli, A., Lavrentovich, O.D., Selinger, J.V.: Physics of liquid crystals of bent-shaped molecules. Rev. Mod. Phys. **90**, 045004 (2018)
3. Daniel, J.C., Audebert, R.: Small Volumes and Large Surfaces: The World of Colloids in Soft Matter Physics edited by M. Williams (Springer-Verlag, Berlin Heidelberg, Daoud and C.E (1999)
4. Chaikin, P.M., Lubensky, T.C.: Principles of Condensed Matter Physics, Cambridge University Press, CambridgeCambridgeCambridge, UK (2000)
5. Comiskey, B., Albert, J., Yoshizawa, H., Jacobson, J.: Nature **394**, 253 (1998)
6. Wang, Z., Zhe, J.: Chip **11**, 1280 (2011)
7. Araki, T., Buscaglia, M., Bellini, T., Tanaka, H.: Nat. Mater. **10**, 303 (2011)
8. Smalyukh, I.I.: Annu. Rev. Condens. Matter Phys. **9**, 207 (2018)
9. Kim, Y.-K., Wang, X., Mondkar, P., Bukusoglu, E., Abbott, N.: Nature **557**, 539 (2018)
10. Nance, E.A., Woodworth, G.F., Sailor, K.A., Shih, T.-Y., Xu, Q., Swaminathan, G., Xiang, D., Eberhart, C., Hanes, J.: Sci. Transl. Med. **4**, 149ra119 (2012)
11. Woltman, S.J., Jay, G.D., Crawford, G.P.: Nat. Mater. **6**, 929 (2007)
12. Poulin, P., Cabuil, V., Weitz, D.A.: Phys. Rev. Lett. **79**, 4862 (1997)
13. Vilfan, M., Osterman, N., Čopič, M., Ravnik, M., Žumer, S., Kotar, J., Babič, D., Poberaj, I.: Phys. Rev. Lett. **101**, 237801 (2008)
14. Ognysta, U., Nych, A., Nazarenko, V., Muševič, I., Škarabot, M., Ravnik, M., Žumer, S., Poberaj, I., Babič, D.: Phys. Rev. Lett. **100**, 217803 (2008)

15. Škarabot, M., Ravnik, M., Žumer, S., Tkalec, U., Poberaj, I., Babič, D., Osterman, N., Muševič, I.: Phys. Rev. E **77**, 031705 (2008)
16. Ryzhkova, A.V., Škarabot, M., Muševič, I.: Phys. Rev. E **91**, 042505 (2015)
17. Lapointe, C.P., Mason, T.G., Smalyukh, I.I.: Science **326**, 1083 (2009)
18. Lapointe, C.P., Hopkins, S., Mason, T.G., Smalyukh, I.I.: Phys. Rev. Lett. **105**, 178301 (2010)
19. Ognysta, U.M., Nych, A.B., Uzunova, V.A., Pergamenschik, V.M., Nazarenko, V.G., Škarabot, M., Muševič, I.: Phys. Rev. E **83**, 041709 (2011)
20. Kim, S.-J., Lee, B.-K., Kim, J.-H.: Liq. Cryst. **43**, 1589 (2016)
21. Andrienko, D., Tasinkevych, M., Patrício, P., Allen, M.P., Teloda Gama, M.M.: Phys. Rev. E **68**, 051702 (2003)
22. Izaki, K., Kimura, Y.: Phys. Rev. E **87**, 062507 (2013)
23. Araki, T., Nagura, J.: Phys. Rev. E **95**, 012706 (2017)
24. Conklin, C., Tovkach, O.M., Viñals, J., Calderer, M.C., Golovaty, D., Lavrentovich, O.D., Walkington, N.J.: Phys. Rev. E **98**, 022703 (2018)
25. Muševič, I.: Nematic liquid-crystal colloids. Materials **11**, 24 (2018)
26. Calderon, F.L., Stora, T., Mondain Monval, O., Poulin, P., Bibette, J.: Phys. Rev. Lett. **72**, 2959 (1994)
27. Yada, M., Yamamoto, J., Yokoyama, H.: Phys. Rev. Lett. **92**, 185501 (2004)
28. Takahashi, K., Ichikawa, M., Kimura, Y.: Phys. Rev. E **77**, 020703(R) (2008)
29. Škarabot, M., Ryzhkova, A.V., Muševič, I.: J. Mol. Liq. **267**, 384 (2018)
30. Pishnyak, O.P., Tang, S., Kelly, J.R., Shiyanovskii, S.V., Lavrentovich, O.D.: Phys. Rev. Lett. **99**, 127802 (2007)
31. Pishnyak, O.P., Shiyanovskii, S.V., Lavrentovich, O.D.: J. Mol. Liq. **164**, 132 (2011)
32. Pagès, Josep M., Ignés-Mullol, Jordi, Sagués, Francesc: Phys. Rev. Lett. **122**, 198001 (2019)
33. Atzin, N., Guzmán, O., Gutiérrez, O.: Phys. Rev. E **97**, 062704 (2018)
34. Denniston, C., Orlandini, E., Yeomans, J.M.: Phys. Rev. E **63**, 056702 (2001)
35. Changizrezaei, S., Denniston, C.: Phys. Rev. E **99**, 052701 (2019)
36. Ravnik, M., Žumer, S.: Liq. Cryst. **36**, 1201 (2009)
37. Ravnik, M.: Liq. Cryst. Today **20**, 77 (2011)
38. Tasinkevych, M., Silvestre, N.M., da Gama, M.M.T.: New J. Phys. **14**, 073030 (2012)
39. Seyednejad, S.R., Mozaffari, M.R., Ejtehadi, M.R.: Phys. Rev. E **88**, 012508 (2013)
40. Chernyshuk, S.B., Lev, B.I.: Phys. Rev. E **81**, 041701 (2010)
41. Chernyshuk, S.B., Lev, B.I.: Phys. Rev. E **84**, 011707 (2011)
42. Chernyshuk, S.B., Tovkach, O.M., Lev, B.I.: Phys. Rev. E **85**, 011706 (2012)
43. D'Adamo, G., Marenduzzo, D., Micheletti, C., Orlandini, E.: Phys. Rev. Lett. **114**, 177801 (2015)
44. Xiao, K., Chen, X., Wu, C.X.: Phys. Rev. Res. **1**, 033041 (2019)
45. Kim, S.-J., Kim, J.-H.: Soft Matter **10**, 2664 (2014)
46. Lee, B.-K., Kim, S.-J., Lev, B., Kim, J.-H.: Phys. Rev. E **95**, 012709 (2017)
47. Frank, F.C.: On the theory of liquid crystals. Faraday Discuss **25**, 19–28 (1958)
48. Rapini, A., Papoular, M.: J. Phys. (Paris), Colloq. **30**, C4–54 (1969)
49. Stark, H.: Phys. Rep. **351**, 387 (2001)
50. Stark, H.: Phys. Rev. E **66**, 032701 (2002)
51. Wang, Y., Zhang, P., Chen, J.Z.Y.: Phys. Rev. E **96**, 042702 (2017)
52. Yao, X., Zhang, H., Chen, J.Z.Y.: Phys. Rev. E **97**, 052707 (2018)
53. Poulin, P., Stark, H., Lubensky, T.C., Weitz, D.A.: Science **275**, 1770 (1997)
54. Poulin, P., Weitz, D.A.: Phys. Rev. E **57**, 626 (1998)
55. Lubensky, T.C., Pettey, D., Currier, N., Stark, H.: Phys. Rev. E **57**, 610 (1998)
56. Senyuk, B., Puls, O., Tovkach, O.M., Chernyshuk, S.B., Smalyukh, I.I.: Nat. Commun. **7**, 10659 (2016)
57. Zhou, Y., Senyuk, B., Zhang, R., Smalyukh, I.I., de Pablo, J.J.: Nat. Commun. **10**, 1000 (2019)
58. Ruhwandl, R.W., Terentjev, E.M.: Phys. Rev. E **54**, 5204 (1996)
59. Ruhwandl, R.W., Terentjev, E.M.: Phys. Rev. E **56**, 5561 (1997)
60. Loudet, J.C., Poulin, P.: Phys. Rev. Lett. **87**, 165503 (2001)
61. Jackson, J.D.: Classical Electrodynamics, 3rd edn. Wiley, New York (1999)